Vilnius University
Faculty of Physics
Institute of Applied Electrodynamics and Telecommunications

Zifan Wang

NOISE SPECTROSCOPY OF HYBRID COMPOSITES WITH CARBON NANOPARTICLES

Master's final thesis
Electronics and Telecommunication Technologies study program

Student	Zifan Wang
Approved	2026-05-22
Academic supervisor	dr. Sandra Pralgauskaitė
Reviewer	dr. Edita Palaimiene
Director of the Institute	dr. Robertas Grigalaitis

Vilnius 2026

Table of Contents

Introduction

In 1971, M.L. Lieberman reported the growth of tubular, twisted, and balloon-like graphitic filaments [1]. Transmission electron microscopy revealed that these low tubes were multi-walled Carbon Nanotubes (MWCNTs). In 1985, Harold Kroto from the University of Sussex, along with James R. Heath, Sean O' Brien, Robert Curl, and Richard Smalley from Rice University, discovered C60, which soon led to the discovery of fullerenes [1]. Fullerenes are a form of carbon that has spurred extensive research into these materials and similar structures, effectively creating a new branch in materials science and nanotechnology.

It has taken time, but interest in materials based on these structures has not only persisted but continues to grow [2]. Finally, in 1991, Al Harrington and Tom Maganas of Magana's Industries discovered the synthesis of nanotubes using Chemical Vapor Deposition (CVD), which led to the development of the method for producing monomolecular thin film nanotube coatings [1].

Nowadays, there is a plethora of carbon nanostructures. Among these, carbon nanotubes stand out due to their unique physical and chemical properties [3]. Carbon nanotubes (CNTs) are used as additives in various primary components, such as tennis rackets and car parts, to enhance the properties of the base material [1]. It is promising to revolutionize several fields of fundamental science and serve as a major component of nanotechnology [3].

Carbon nanotubes possess numerous excellent properties, including high electrical conductivity and high current density. However, it has been observed that their exceptional performance is closely linked to noise characteristics. Low-frequency (flicker) noise is a critical parameter for nearly all electronic devices. It holds particular significance for high-frequency applications as it determines the Noise Equivalent Power (NEP) of detectors and the phase noise of high-frequency generators and mixers. Low-frequency noise holds particular significance for devices employing carbon nanotubes, which serve as fundamental building blocks for a variety of sensors, including radio frequency and terahertz detectors [4].

The aim of this research is to investigate the resistance and low frequency noise characteristics of composites with single-walled and multi-walled carbon nanotubes.

This work is continuous: Zifan Wang resistivity and low frequency noise characteristics of composites with carbon nanotubes of varying sizes Master's scientific research work Electronics and Telecommunication Technologies study program 2024.

1. Carbon Nanostructures

This is the first section of the literature review that will focus on the object of this study: carbon nanotube composites.

1.1. Carbon Nanotubes

Carbon nanotubes (CNTs) consist of one or more seamless cylindrical shells of graphitic sheets. Each shell is made of (trivalent) carbon atoms forming a hexagonal network without any edges. Essentially, a nanotube can be conceptualized as a tubular microcrystal of graphite [5].

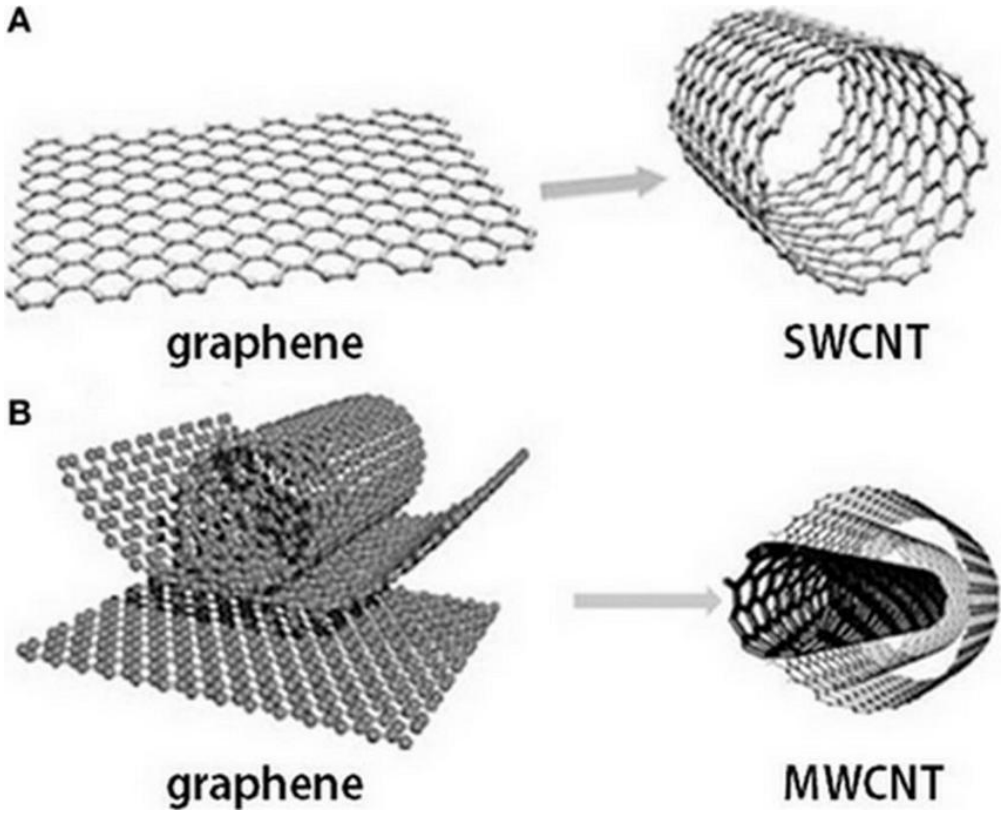

Figure 1.1.1. Different types of CNTs based on their number of graphene cylinders: (a) capped single-wall CNT (SWCNT); and (b) open multi-wall CNT (MWCNT) [1].

Based on their structure, carbon nanotubes are classified as single-wall (SWCNT) or multi-wall (MWCNT). Single-walled carbon nanotubes are the seamless cylinders of one layer of graphene which itself is a hexagonal arrangement of carbon atoms in one plane. Multi-wall carbon nanotubes are multiple layers of graphene rolled up with an interlayer distance of 330 pm. The difference between single-wall carbon nanotubes and multi-wall carbon nanotubes is displayed in Figure 1.1.1.

Carbon nanotubes possess several unique and desirable properties. One of the most remarkable is the ability to combine high flexibility and strength with high stiffness, a characteristic not found in graphite fibers. Additionally, their excellent conductivity and capacity to carry high current density, coupled with high thermal conductivity, render them highly desirable for electronics applications [6].

A comparison of the characteristics of SWCNTs and MWCNTs is given in Table 1. The key differences to highlight are resistivity and tendency to agglomerate. Single-walled carbon nanotubes (SWCNTs) typically have lower resistivity compared to multi-walled carbon nanotubes (MWCNTs), but they are harder to disperse [1].

Table 1.1.1. Comparison between SWCNTs and MWCNTs [1].

SWCNT	MWCNT
Single layer of graphene.	Multiple layers of graphene.
Catalysts are required for synthesis.	Can be produced without catalyst.
Bulk synthesis is difficult as it requires proper control overgrowth and atmospheric condition.	Bulk synthesis is easy.
Not fully dispersed, and form bundled structures.	Homogeneously dispersed with no apparent bundled formation.
Resistivity is usually in the range of $10^{-4} - 10^{-3}\ \Omega m$.	Resistivity is in the range of $1.8 \times 10^{-5} - 6.1 \times 10^{-5}\ \Omega m$.
Purity is poor.	Purity is high.
The chance of defect is more during functionalization.	The chance of defects is less especially when synthesized by arc-discharge method.
Characterization and evaluation is easy.	It has very complex structure.
It can be easily twisted and are more pliable.	It cannot be easily twisted.

In recent years, many advanced technologies to fabricate carbon nanotubes have been developed. There are several methods to fabricate CNTs. Methods of note include:

- Arc discharge methods can produce both multi-walled carbon nanotubes (MWCNTs) and single-walled carbon nanotubes (SWCNTs) when carbon vapors cool and condense. Typically, MWCNTs are formed in the absence of catalyst particles between two graphite electrodes, while SWCNTs can be generated by introducing catalysts such as Fe, Ni, or Co. These catalysts can be introduced by packing metal powder into a hole in the anode. As the metal is

consumed along with the graphite, catalyst particles are created, favoring the formation of small-diameter SWCNTs [4].

- Chemical vapor deposition (CVD) is another method for synthesizing carbon nanotubes. Catalytic CVD synthesis involves placing a carbon source in the gas phase and using plasma or a resistively heated coil to heat the gaseous carbon-containing molecules. This heat "cracks" the molecules into reactive atomic carbon. The most commonly used catalysts in this process are transition metals, primarily Fe, Co, or Ni [4].

- The laser ablation method utilizes both pulsed and continuous lasers to vaporize a graphite target in an oven. The oven is filled with helium or argon gas to maintain pressure [4].

1.2. Carbon Nanotube Composites

CNT/polymer composites are a composite material formed by dispersing carbon nanotubes (single-wall or multi-wall) into the polymer matrix. Like carbon nanotubes, CNT/polymer composites also has superior performance. Moreover, we can change its performance by changing filler concentration, the processing method and type of polymer matrix to meet our special needs. From [7], it summarizes many articles, showing that different characteristics are obtained by changing the CNT/polymer composites filler concentration, the processing method, and the type of polymer matrix. For example, in terms of mechanical performance, when matrix is PS, the filler is Purified MWCNTs, and the processing method of solution casting is used, when the CNT weight is 1 wt.%, the tensile strength of polymer composites increase by 25%, Young modulus increase by 42%, and when the CNT weight is 5 wt.%, the tensile strength of the polymer compositions increase by 50%, and Young modulus increase by 120%. As far as electrical performance is concerned, when matrix is PS, the filler is SWCNTS, and the processing method of the solution mixing is used. When the CNT weight is 2 wt.%, the electrical conductivity of the polymer composites is $10^{-3}\ S/m$, and when the CNT weight is 1.5 wt%, the electrical conductivity of polymer composites is $1\ S/m$. When the matrix type and the processing method remain unchanged, the CNT weight is 1.5 wt%, the electrical conductivity with SWCNTs is $10^{-3}\ S/m$, the electrical conductivity of PMPV-Coated SWCNTs is $2 \times 10^{-7}\ S/m$.

From the above, it is evident that the electrical properties of binary mixtures are heavily influenced by the microstructure. Specifically, factors such as dispersion state, filler geometry, and filler-matrix interactions play a significant role in shaping the electrical properties of nanocomposite materials [8]. Moreover, several studies indicate that the percolation threshold and conductivity are greatly influenced by factors such as the type of polymer and synthesis method, the aspect ratio of

CNTs, the dispersion of CNT agglomerates, the uniform spatial distribution of individual CNTs, and the degree of alignment [7].

Since the fabrication has a great influence on its properties, the commonly used methods for fabricating polymers are listed here as follows:

- The direct growth of graphene nanoflakes (GNFs) on carbon fibers using microwave plasma-enhanced chemical vapor deposition (CVD) [9].

- Melt mixing: in this method, filler particles are mixed with a molten polymer and the mixture is cooled in a mold. For example, a mixture of PANI-ES and DBSA in a weight ratio of 1:0.5 was dissolved in xylene to prepare PANI dispersions (quasi-solutions) ranging from 5 to 9 wt.%. These solutions were vigorously stirred for 3 hours at 90°C, followed by treatment in an ultrasonic bath for 2 hours [8]. The process typically entails blending polymers with CNTs, often at high filler contents, either continuously or in batch form, at a specific temperature using an extruder or a high-shear mixer [10].

- Solution mixing: CNTs are dispersed in a suitable solvent by stirring, mixing, or sonication, where mechanical energy is applied to unbundle the CNTs. Subsequently, the dispersed CNTs are mixed with a polymer, followed by a controlled evaporation process. Finally, the dispersed CNTs and polymer matrix are blended to form a composite film [10].

- Sonication: during sonication, as the CNT bundles break down into individual CNTs, the dispersing molecules adsorb onto the surface of the CNTs [10].

- Resin transfer molding: CNTs are drawn from super-aligned arrays and joined end-to-end by Van der Waals forces, resulting in the creation of a continuous and aligned CNT sheet. The process of making a CNT preform involved stacking CNT sheets together at various orientations, followed by inserting the preform into the resin transfer mold. Subsequently, the sealed resin transfer molding mold was injected with liquid epoxy resin, which fully infiltrated the CNT preform in a vacuum oven. Upon increasing the oven temperature to cure the epoxy, a CNT/epoxy composite aligned in a solid state was formed. After cooling the resin transfer mold to room temperature, it was released from the CNT/epoxy composite sample. The properties of the composites may vary depending on the type of CNT preforms and resin transfer molds used [10].

1.3. Hybrid Carbon Nanotube Composites

The development of hybrid carbon nanotube composites involves incorporating various types of fillers into a single matrix. By using a hybrid composite containing two or more types of fillers, the advantages of one filler type can complement the shortcomings of another [11].

Hybrid carbon nanotube composites hold significant promise and are extensively discussed due to the synergy effect they exhibit. An illustrative example of this theory is evident in cases where the ratio of reduced graphene oxide (rGO) to single-walled carbon nanotubes (SWNTs) is 1:1. This results in the formation of an interconnected network that aligns closely along the fiber. Within this structure, rGO nanosheets are preferentially oriented in the fiber direction, with SWNT bundles attached to the edges and surfaces of the rGO. The high degree of self-alignment achieved during spinning offers the potential for remarkable toughness [12].

1.4. Charge Transfer in Carbon Nanotube Composites

When discussing charge transfer in carbon nanotube composites, the following three phenomena are important to note. Firstly, the percolation process refers to the transport of current in a disordered system with localized states. This transport is realized through the hopping of electrons from one state to another [13]. The percolation threshold is defined as the critical filler fraction of the polymer at which it transitions from an insulating state to a conductive state [14]. The changes of material when the percolation process is shown in Figure 1.4.1.

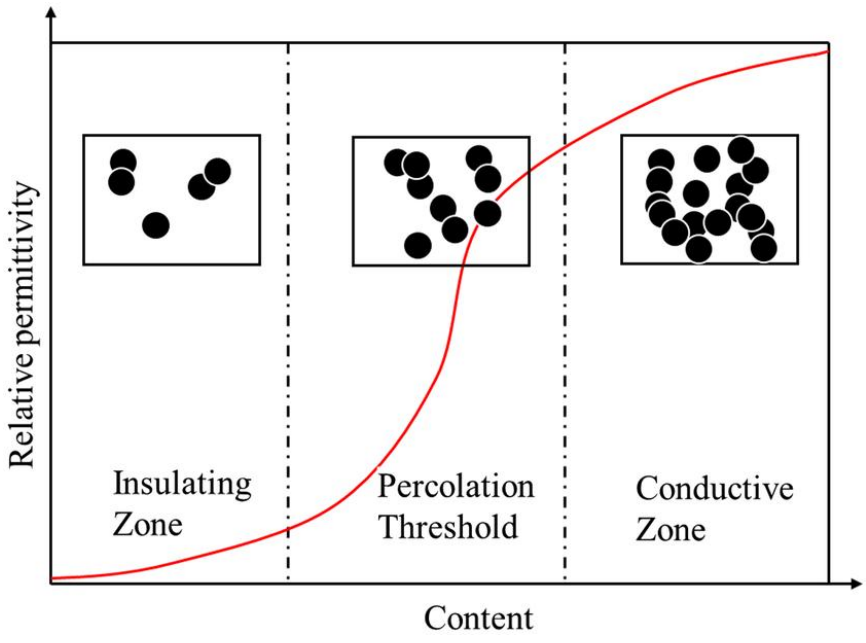

Figure 1.4.1. Conductivity of filled CPCs vs. addition of conductive materials [14].

The given equation describes the relationship between electrical conductivity of the materials and the conductivity of the fillers, the percolation threshold, and the volume fraction:

$$\sigma = \delta(p - p_c)^t \quad 1.1$$

Where σ is the polymer composite's conductivity, δ is the conductivity-related constant of the conducting material, p is the mass fraction of the conducting material, p_c is the polymer composite percolation threshold, and t is the conductive network dimensionality critical factor.

Secondly, at the limit of absolute zero temperature, the contact resistance represents the quantum tunnelling resistance of electrons. As the temperature increases, there is an intermediate temperature regime for quantum tunnelling known as thermally assisted tunnelling, which occurs due to the excited levels of tunnelling across the barrier. The transport of electrons over the polymer barrier is predominantly governed by thermally activated hopping, following the Arrhenius law. The distinction between thermally assisted tunnelling and thermally activated hopping lies in the fact that tunnelling occurs at excited energy levels between the bottom and top of the barrier, whereas hopping always occurs at the top of the barrier [15].

Here, variable range hopping is defined by Mott's law:

$$\rho_{\text{mott}} = \rho_0 exp\left(\frac{T_0}{T}\right)^{\frac{1}{d+1}} \quad 1.2$$

whereρ_0 is the resistance parameter, T_0 is the temperature parameter, T is the absolute temperature and *d* is the spatial dimension coefficient [16].

Thermal activation is defined by the Arrhenius' law:

$$\rho_{\text{Arr}} = \rho_0 exp\left(\frac{\Delta E}{K_B T}\right) \quad 1.3$$

where ρ_0 is the resistance parameter, ΔE is the activation energy, K_B is the Boltzmann constant and T is the absolute temperature [16].

2. Electric Noise in Carbon Nanotube Composites

This is the second section of the literature review that will focus on different types of noise that can be observed in carbon nanotube composites.

2.1. 1/*f* Noise

The name "flicker noise" refers to noise phenomena with a spectrum of the form AI^{β}/f^{γ}, where A is a constant, I is the current, f is the frequency, and the exponents β and γ are also constants [17]. For Low-frequency noise, the spectral density depends inversely on frequency [18].

In recent years, there has been extensive discussion regarding the source of flicker noise, with the prevailing consensus now accepting the following statement: avalanches formed in plasma can account for the occurrence of flicker noise [19].

Since flicker noise has a huge impact on our signals and devices, understanding its mechanism can help us better solve problems that arise in signals and devices. Below I have listed a few points about how it affects the device's sensors:

- The stability of laser sources will be influenced since laser sources must be frequency stabilized for interferometric measurements with high accuracy [20].
- Low-frequency noise potentially has a significant impact on the phase noise of nonlinear circuits and devices operating in the GHz region [21].
- The inherited error in N will accumulate over time, contributing to a nontrivial amount of error in the SEIR algorithm. This accumulation will cause a drift in the constant offset between the two ramps [22].

At the same time, it also has a great impact on materials. The flicker noise, which manifests itself at low-frequencies (usually 0.01 kHz – 100 kHz) with the $1/f^{\gamma}$ spectral density dependence, is an important figure-of-merit for semiconductor devices since this type of noise is the limiting phase-noise factor for all kinds of transistors (γ is a parameter close to 1) [23]. Measuring the flicker noise of the material can characterize the material quality, which can help us choose the best material for the device.

2.2. Generation–Recombination Noise

Generation-recombination (GR) noise arises from fluctuations in the number of free carriers within a two-terminal sample, resulting from random transitions of charge carriers between states in different energy bands. As a result, GR noise is fundamentally caused by fluctuations in carrier number, typically maintaining charge neutrality across the total sample [24].

Generation–recombination noise is observed at low f and its spectral density is described by the Lorentzian: $S_{\mathrm{I}}(f) = S_0/[1 + (2\pi f\tau)^2]$, where S_0 is the frequency independent portion of $S_{\mathrm{I}}(f)$ observed at $f < (2\pi f\tau)^{-1}$ and τ is the time constant associated with a specific trapping state (for example, ionized impurity) [18].

2.3. Thermal Noise

Thermal noise originates from the random thermal motion of electrons within the circuit [26]. Additionally, both thermal and shot noise types arise from the random motion of charge carriers. They are referred to as white noise because their spectral density remains constant across frequencies [18].

The spectral density of thermal noise is given by Nyquist's formula:

$$S_{\mathrm{I}}(f) = 4K_{\mathrm{B}}TR \qquad 2.1$$

where k_{B} is Boltzmann's constant and T is temperature, R is resistance [25].

Based on its origin, we understand that thermal noise is inevitable at typical temperatures, except when the conductor is cooled to cryogenic temperatures [26].

2.4. Shot Noise

Shot noise arises from the discrete nature of charge carriers in electronic devices [17]. The spectral density of shot noise does not depend on frequency [25]. For instance, in a superconductor, the magnetic field divides into elementary fluxoids. When current flows, a Lorentz force acts on these fluxoids, causing them to move uniformly across the foil and induce voltage pulses between the probe contacts. Since fluxoids randomly appear and disappear on opposite sides of the foil, their motion creates shot noise.

2.5. Noise in Carbon Nanotube Composites

Tretjak et. al. [2] studied the low frequency noise of multi-wall carbon nanotube (MWCNT) and onion-like carbon (OLC) epoxy resin composites, and found that the primary noise type was flicker type. This flicker type noise in these composites was found to originate from a superposition of generation and recombination processes that lead to the fluctuating number of the free charge carriers in the composite.

Collins et. al. [27] also studied the excessive noise in a single nanotube (SWCNT) device, and found that the SWCNT device demonstrates the excessive flicker noise. They found that electrical barriers at nanotube-nanotube junctions product fluctuations with a *1/f* power spectrum measured by four-probe.

Merchant et. al. [28] studied the shot noise measurements in a carbon nanotube-based spin diode, and they gave a representative plot of the current noise, S, as a function of frequency for several bias voltages for a fixed gate voltage, found that when the frequencies above ~ 20 kHz, the shot noise was dominant, which depends strongly on the gate voltage. Furthermore, they saw a significant periodic reduction in the current shot noise, though that may be due to increased spin-flip rates at certain gate voltages.

Chaste et. al. [29] studied thermal shot noise in top-gated single carbon nanotube field effect transistors and they supported the thermal noise of generalized Johnson – Nyquist expression in 1D transistors.

3. Studied Composite Sample Characteristics

In this work, the study was divided into two parts. In part one, composite samples containing a mix of single-wall and multi-wall carbon nanotubes were studied. The concentration of both types of filler in the material was 0.5 wt.%. The dimensions, resistivity and load resistance magnitude are given in Table 3.1.

Table 3.1. Characteristics of composite samples with 0.5 wt.% SWCNT and 0.5 wt.% MWCNT.

Sample	Dimensions, mm	Resistivity ρ, Ωm	Sample resistance R, kΩ	Load resistance R_{load}, kΩ
1A	4.72 × 5.52 × 1.55	18.33	1.01	18.27
1B	5.14 × 5.22 × 2.42	17.75	1.60	18.27
1C	8.83 × 5.06 × 2.40	18.19	1.63	18.27 and 194.2
2A	5.43 × 4.05 × 2.10	47.89	4.57	83.37
2B	6.06 × 4.59 × 1.37	71.27	3.51	83.37
2C	7.60 × 5.71 × 2.40	172.26	9.53	83.37 and 194.2

In part two, composite samples contained single-wall or multi-wall carbon nanotubes, but the concentration of these types of filler in the material were different. The concentrations were given in Table 3.2.

Table 3.2. Parameters of the composite samples with different concentrations of filler (U = 9.2 V).

Sample	SWCNT, wt.%	MWCNT, wt.%	Dimensions, mm	Resistivity ρ, Ωm	Load resistance R_{load}, kΩ
2SW	2	-	4.30 x 3.80 x 1.65	2.43	18.27
1SW-1MW	1	1	5.32 x 2.47 x 1.65	6.10	18.27
1SW	1	-	5.15 x 5.20 x 2.23	8.63	18.27
0.5SW-0.5MW	0.5	0.5	8.83 x 5.06 x 2.40	18.19	18.27 and 194.2

Composite samples for this study were provided by dr. Jan Macutkevič. Samples were produced using melt processing of the polymer polydimethylsiloxane (PDMS) and the CNT fillers. Alcohol solvent and filler suspensions were made, mixed for 30 minutes and then sonicated for 2 hours to disperse. PDMS base was added to the suspensions and sonicated again for 3 hours until

the solvent evaporated. The PDMS curing agent is then added and the mixture is transfered to a mould, and heated at 100 °C for 40 minutes.

The polydimethylsiloxane *SYLGARD 184* was used [30]. Commercially available SWCNT and MWCNT fillers, purchased from US Research Nanomaterials, were fabricated via the CVD method [31][32]. The average length of the SWCNTs is 15-50 μm, with an average diameter of 1.1 nm [31]. The average length of the MWCNTs is 10-30 μm, with an average inner diameter of 5-10 nm and outer diameter of 10-20 nm [32].

In part one of the study, a total of six composite samples were investigated. They are split into two groups: Group 1 (samples 1A, 1B, 1C) and Group 2 (samples 2A, 2B, 2C). Group 1 samples were obtained from the cross-section perpendicular to the bottom of the material. Group 2 samples were obtained from the top surface of the composite. This was done to investigate whether or not the site from which the composite sample is produced has any sort of effect on the sample properties. In both cases, contacts were formed on the surface of the composite by using silver paste.

In part two of the study, a total of four composite samples were investigated. All investigated samples were obtained from the cross-section perpendicular to the bottom of the material. Contacts were also formed on the surface of the composite by using silver paste.

4. Research Methodology

In this section, the research methodology of the resistivity and low frequency noise of composites with CNTs is described.

The experiments were conducted at room temperature to measure the resistivity and noise characteristics. Room temperature measurements of sample voltage to calculate resistivity were performed in two ways: using a semiconductor devices analyser Keysight B2901 or a digital multimeter. The frequency range of the voltage fluctuations at room temperature is 100 Hz to 20 kHz. The noise measurements were carried out with a special chamber to avoid parasitic electromagnetic radiation. And a simplified noise measurement scheme is shown in Figure 4.1. The noise signal was recorded by a personal computer (PC).

For temperature measurements, composite samples are put in a thermally insulated chamber to investigate the resistivity and noise characteristics dependence on temperature. The chamber is cooled by pouring liquid nitrogen, and then the sample is heated using a built-in coil. Lastly, the temperature is measured using a thermistor inside the chamber. The noise signal was also recorded by a personal computer (PC). During temperature characteristic measurements, the total voltage is set to a constant value, and a multimeter is used to measure composite sample voltage, which is then used to calculate the specific resistance.

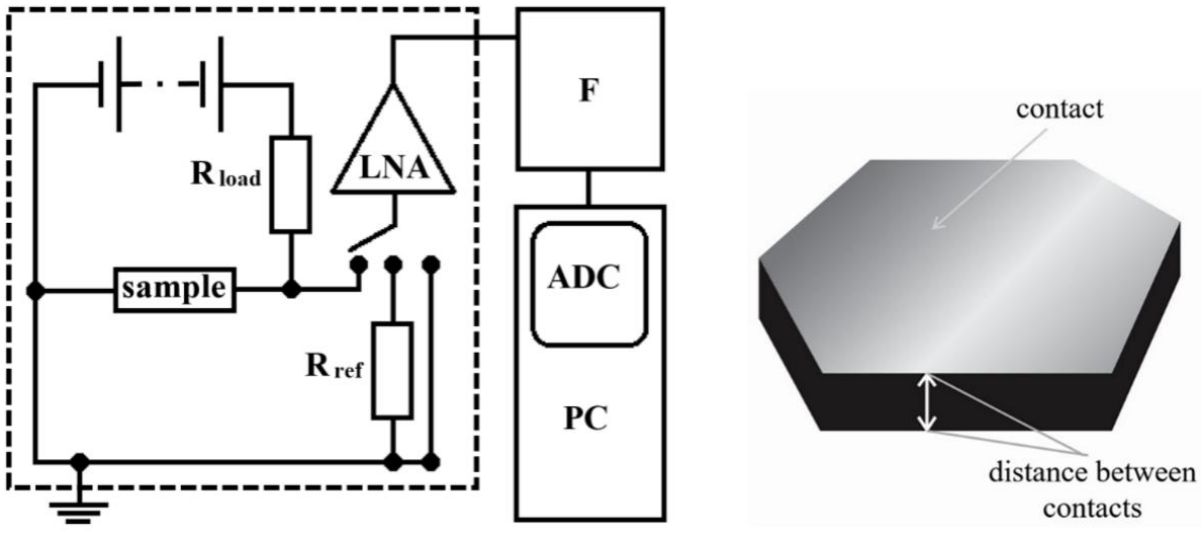

Figure 4.1. Scheme of the noise measuring system (on the left): low noise amplifier (LNA), filter system (F), analog-to-digital converter (ADC), personal computer (PC) and schematic picture of the sample (on the right) [2].

The following equation is used to calculate the spectrum density:

$$S_{\mathrm{U}} = \frac{U^2 - U_{\mathrm{S}}^2}{U_{\mathrm{ref}}^2 - U_{\mathrm{S}}^2} 4k_{\mathrm{B}} T R_{\mathrm{ref}} \qquad 4.1$$

where U^2, U_{ref}^2 and U_{S}^2 are the voltage fluctuations of studied sample (including the noise of the measuring system), of the reference resistor (also including the noise of the measuring system) and of the measuring system in a narrow frequency band sample voltage respectively. T is the absolute temperature of the reference resistor (290 K), R_{ref} is the resistance of the reference resistor and k_{B} is Boltzmann's constant. The values of R_{load} used during a given composite sample's study are given in Tables 3.1 and 3.2. During the first part of the study, the value of the reference resistor R_{ref} was 9.7 kΩ, and during the second part, the value of the reference resistor R_{ref} was 6.7 kΩ. To clarify, the reference resistance value changed because a different amplifier was used.

5. Results

This chapter contains the analysis of the results of the investigation: composite sample resistivity and low frequency noise characteristics.

5.1. Part One: Composite Samples of Varying Size and Region

This section details the results obtained during the first part of the study, where all composite samples have the same filler concentration (0.5 wt.% SWCNT and 0.5 wt.% MWCNT), but are of varying size, and are produced from two different regions of the material.

5.1.1. Resistivity Characteristics

Composite sample specific resistance dependencies on voltage, measured with multimeter, are shown in Figure 5.1.1. Figure 5.1.1 highlights that the specific resistance of sample 2C most strongly depends on the applied voltage. At 4.5 V, its specific resistance is close to 210 Ωm, and at 55 V, it is close to 90 Ωm, decreased by more than 100 %. The specific resistance of other samples slightly depends on the applied voltage.

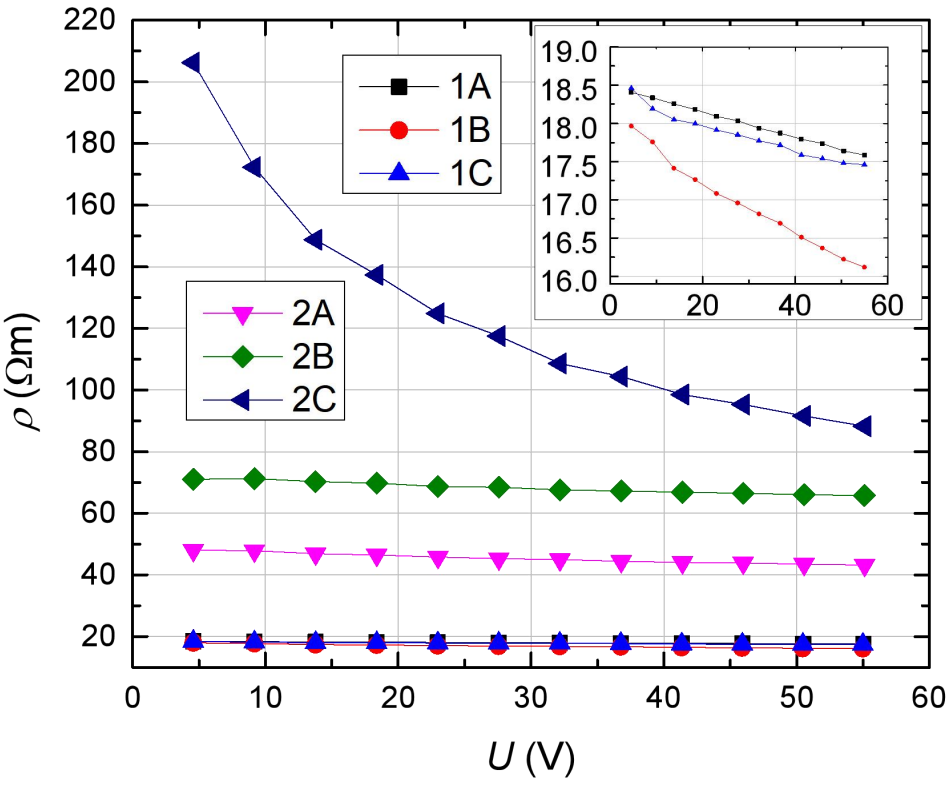

Figure 5.1.1. Dependence of the specific resistance on the applied voltage at room temperature. Inset shows a comparison of composite samples 1A–C.

The size of the composite samples has a great impact on their specific resistance. It can be observed that composite samples from Group 2 have higher specific resistances than samples from Group 1. Specific resistances of 2A, 2B, 2C are respectively close to 50 Ωm, 70 Ωm and 210 Ωm. Meanwhile, the specific resistances of samples 1A, 1B, 1C are roughly the same, close to 20 Ωm. This is possibly due to the material region that they were obtained from. During the solidification process of the material, it is possible that the viscosity of the polymer is not enough to maintain the distribution of carbon nanotubes, and so more carbon nanotubes precipitate at the bottom due to gravitational forces. As a result, less conductive filler particles remain at the top of the material, leading to higher and more varied specific resistance values in Group 2.

5.1.2. Voltage Fluctuations at Room Temperature

For low frequency noise, characteristic examples of noise spectra have been selected for Samples 1C and 2C, with four different applied voltages to show the dependence of the voltage noise spectral density on the different frequency at room temperature have been selected, as shown in Figure 5.1.2 and Figure 5.1.3. The composite sample low frequency noise is predominantly 1/*f* (flicker noise) type. Generally, it can be seen that the noise spectral density of both composite samples decreases with increasing frequency and increases with the increase of the applied voltage.

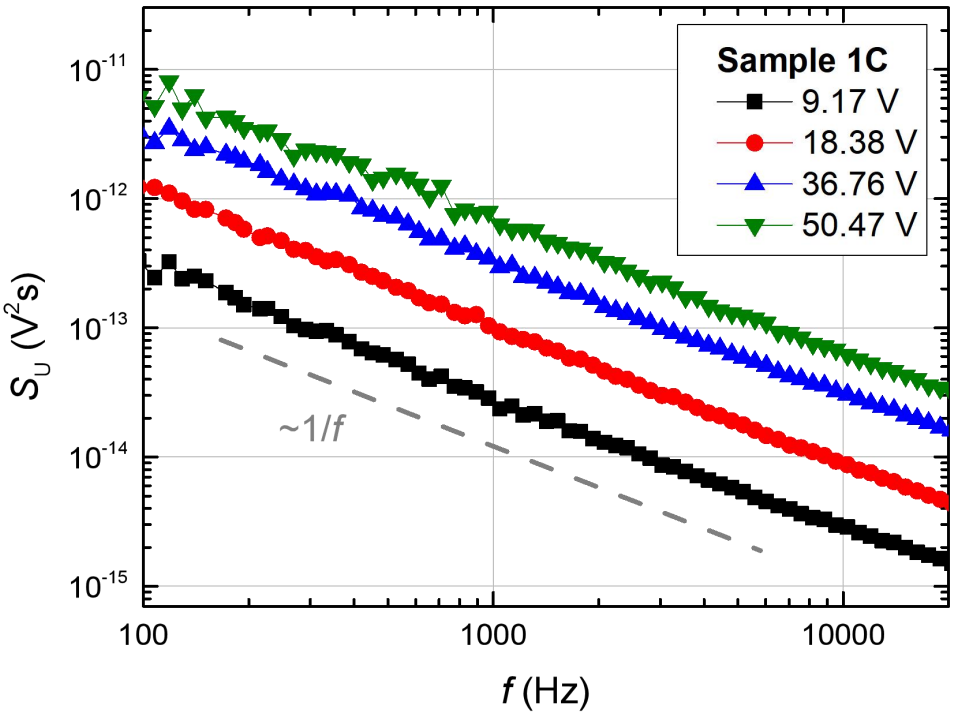

Figure 5.1.2. Dependence of the voltage noise spectral density on the different frequency at room temperature (Sample 1C).

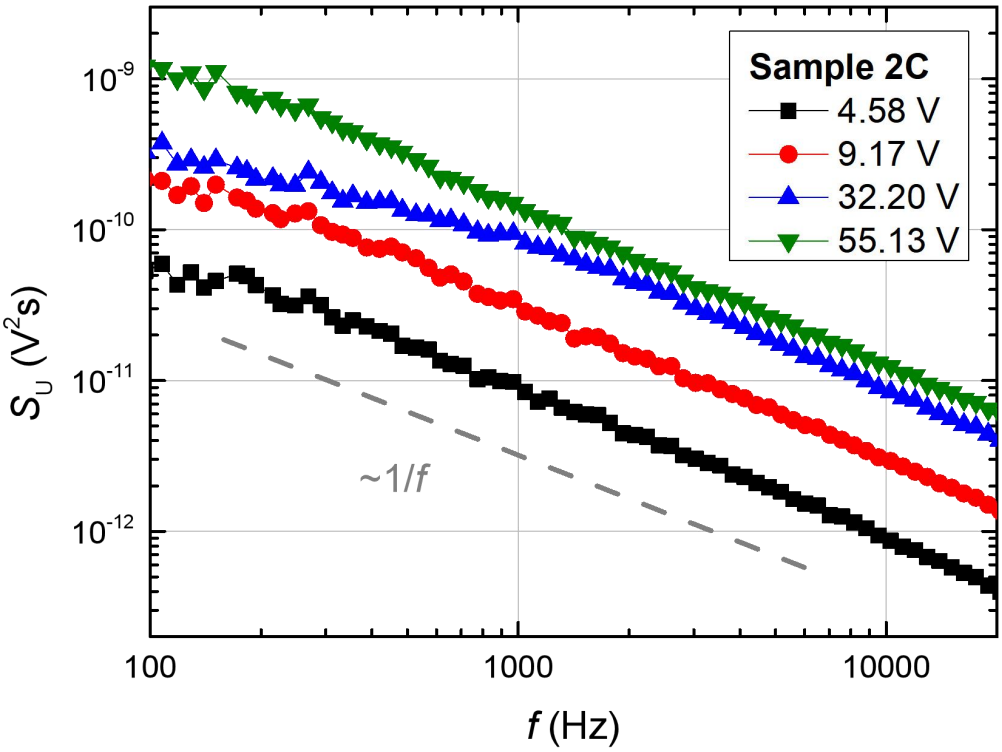

Figure 5.1.3. Dependence of the voltage noise spectral density on the different frequency at room temperature (Sample 2C).

The voltage noise spectral density is proportional to the exponent of the voltage: $S_U \sim U^b$, where $1 < b < 2$. The exponent $b = 2$ is characteristic of resistance fluctuations due to processes of generation and recombination of charge carriers. In Figure 5.1.4, the values of S_U are normalized, so by observing the initial slopes of all samples, one can see that the exponent b values are close to 2. This relationship means that the spectral density of noise increases quadratically with increasing sample voltage, and the changes are related to resistive fluctuations in the material, which means the noise due to the generation and recombination of charge carriers inside the material.

As the sample voltage increases, a change in the slope can be observed , as the exponent b is lower than 2. This relationship means that the spectral density of noise increases more linearly with increasing sample voltage. This situation is often related to tunneling in the material, so tunneling may cause a linear increase in the noise spectral density as the sample voltage increases.

Composite samples from Group 2 show a higher noise intensity than samples from Group 1. By looking at composites from Group 1, one can see that their voltage noise spectral density approaches the same level as the applied voltage increases.

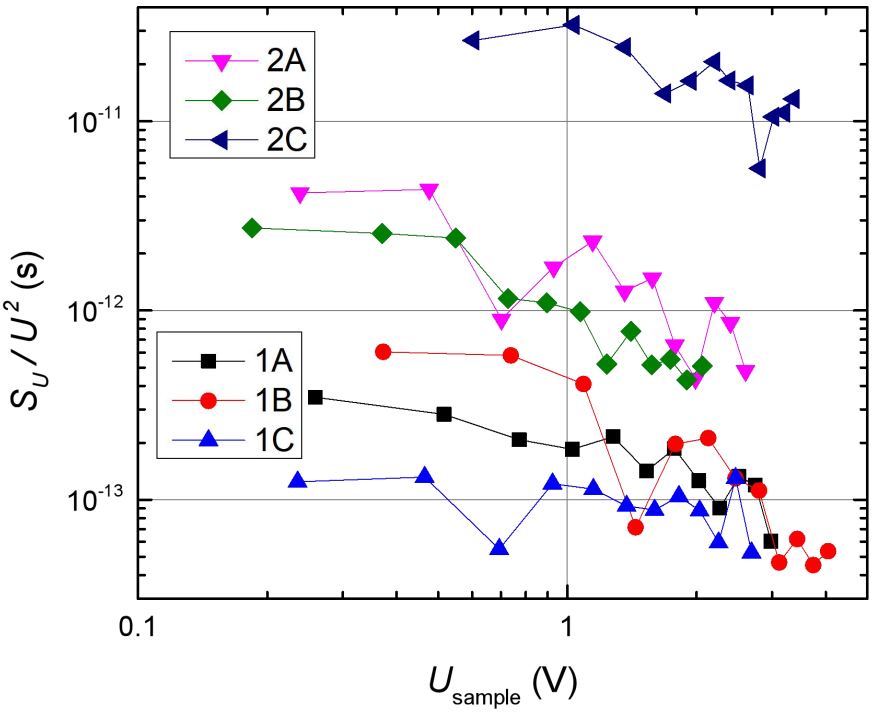

Figure 5.1.4. Dependence of normalized voltage noise spectral density on voltage at room temperature (968 Hz).

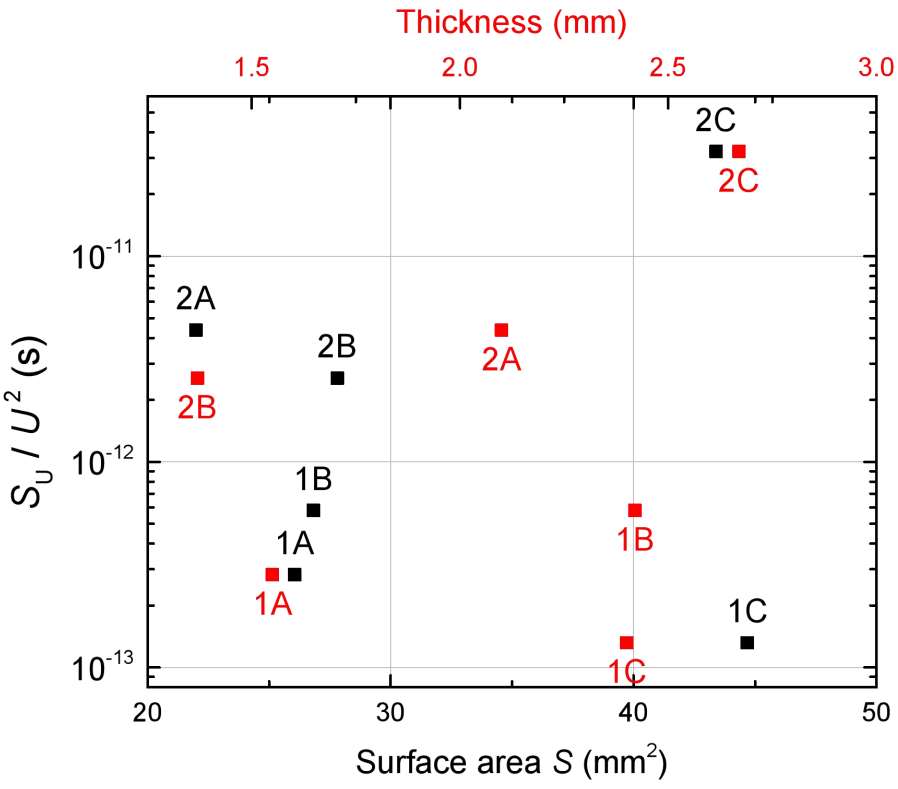

Figure 5.1.5. Dependence of noise level on sample surface area and thickness (968 Hz, U = 9.2 V).

The dependence of noise level on sample surface area and thickness is shown in Figure 5.1.5. Here, the dependency is shown at a frequency of 968 Hz, and the applied voltage is 9.2 V. According to it, it can be observed that the surface area and thickness of the composite sample affects its noise level, though at the current sample count clear trends are generally not visible. The most apparent relation that can be seen is the dependence between noise level and sample thickness (red points) for composite samples from Group 2, where one can see that thicker samples from this group have higher noise.

5.1.3. Characteristics Dependence on Temperature

Based on the results of the room temperature study, two samples 1C and 2C with the biggest difference have been selected to study the resistivity and noise characteristics dependence on temperature under a constant voltage ($U = 9.2$ V).

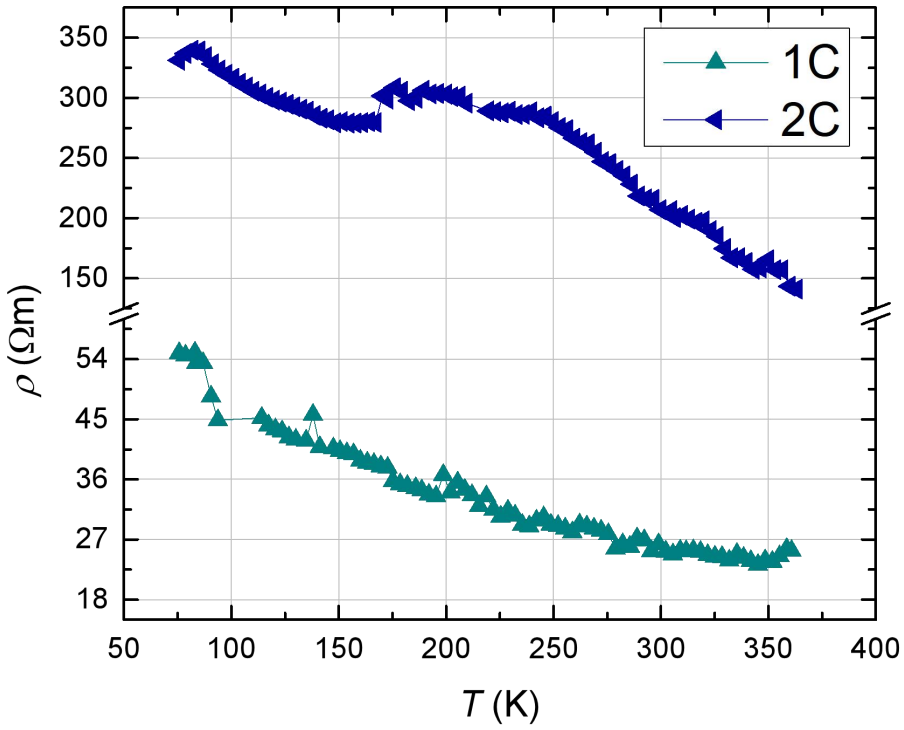

Figure 5.1.6. Dependence of specific resistance of sample 1C and 2C on temperature ($U = 9.2$ V).

The dependence of specific resistance of composite samples 1C and 2C on temperature are shown in Figure 5.1.6. For these two samples, specific resistance is inversely proportional to the temperature. From the figure it can intuitively be observed that the two samples are different characteristics. From the change range of specific resistance, as the temperature increases, the

specific resistance of sample 1C decreases from 54 Ωm to 23 Ωm, with a change range of 31 Ωm, while the specific resistance of sample 2C decreases from about 350 Ωm to about 150 Ωm, with a change range of 200 Ωm, which shows a greater change. Moreover, the descending curve of sample 2C is more fluctuating than that of sample 1C. It can be seen that when the temperature approaches 175 K, the specific resistance of sample 2C increases slightly, and although the specific resistance of sample 1C also shows a slight increase in several temperature ranges, it is flatter than sample 2C.

For low frequency noise, I chose these two samples (1C and 2C) with several most representative temperatures to show the dependence of the voltage noise spectral density on the different frequency at room temperature, as shown in Figure 5.1.7 and Figure 5.1.8. As a whole, these also present that composite sample low frequency noise is predominantly 1/*f* (flicker noise) type. However, looking at the details, it is shown in Figure 5.1.7 that when the temperature is 83.8 K, generation and recombination noise dominates in sample 1C. Similarly, in Figure 5.1.8, when the temperature is 85.0 K, in sample 2C, generation and recombination noise dominates. Generally, it can be seen that the noise spectral density of both samples decreases with increasing frequency.

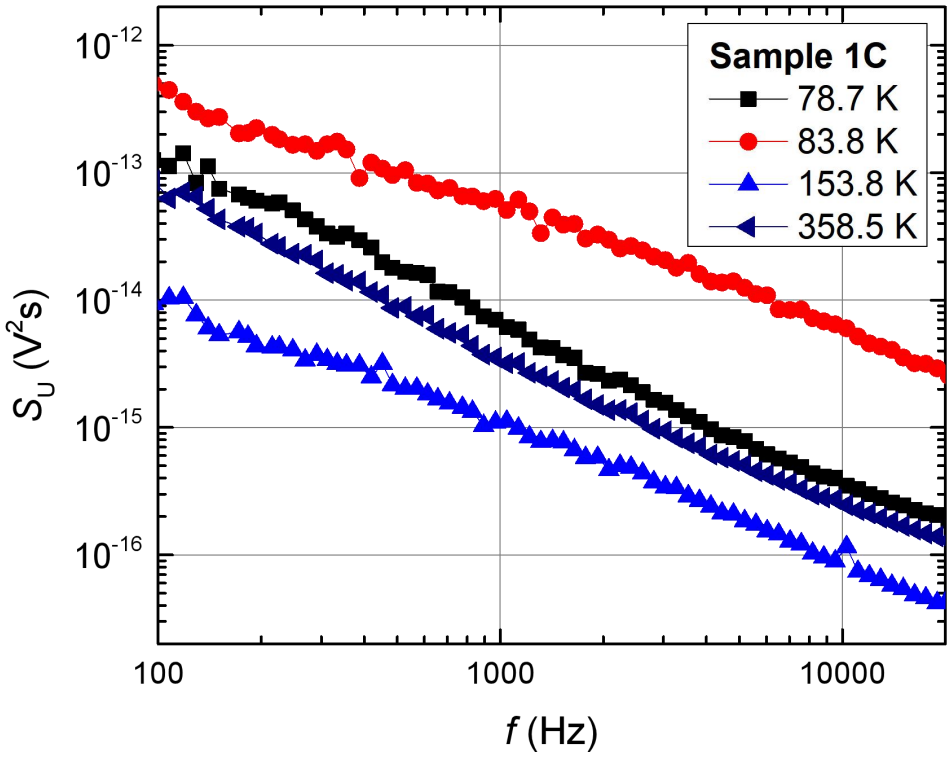

Figure 5.1.7. Dependence of voltage noise spectral density on temperature (sample 1C, $U = 9.2$ V).

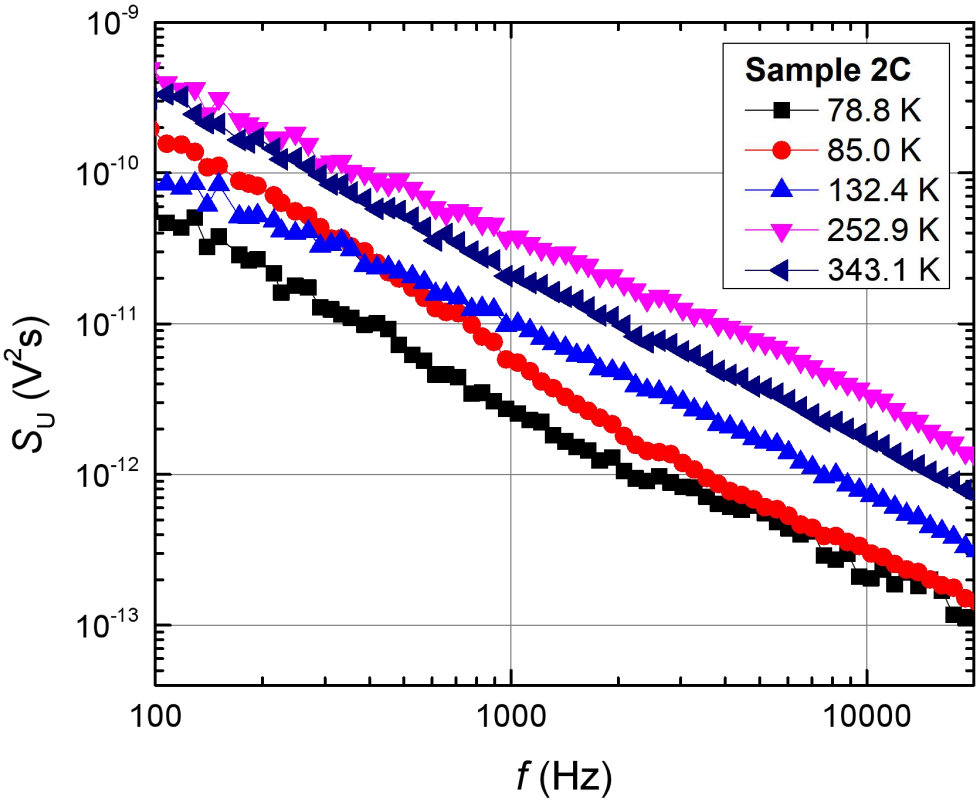

Figure 5.1.8. Dependence of voltage noise spectral density on temperature (sample 2C, U = 9.2 V).

Figure 5.1.9 demonstrates the dependence of normalized voltage noise spectral density of sample 1C and 2C on temperature (968 Hz). Obviously, from the figure it can be seen that the normalized voltage noise spectral density of sample 1C and sample 2C is proportional to the temperature and furthermore, consistent with the conclusions of previous studies, sample 2C has higher normalized voltage noise spectral density than sample 1C. However, it is interesting to note that unlike Figure 5.1.6 which shows that sample 2C has a larger fluctuation in the dependence of specific resistance on temperature, Figure 5.1.9 shows that sample 1C has a larger fluctuation in the dependence of normalized voltage noise spectral density on temperature (968 Hz) compared to sample 2C, indicating that the noise of 1C has more the generation and recombination of charge carriers inside the material.

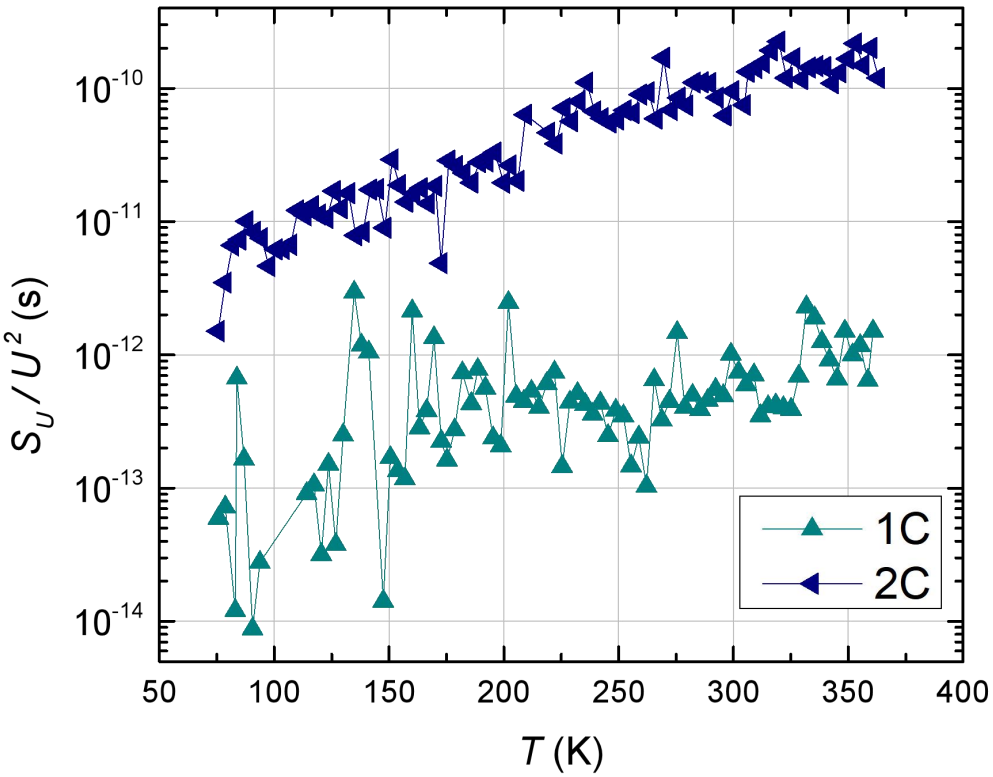

Figure 5.1.9. Dependence of normalized voltage noise spectral density on temperature (968 Hz).

5.2. Part Two: Composites with Varying Concentration of Filler

This section details the results obtained during the second part of the study, where the composite samples have the different filler concentrations.

5.2.1. Resistivity Characteristics

The composite sample specific resistance dependence on voltage is shown in Figure 5.2.1. According to this figure, It can be seen that the specific resistance is inversely proportional to the applied voltage for all samples. This effect is slightly more pronounced for the hybrid SWCNT/MWCNT composites, and least pronounced for the composite sample 2SW.

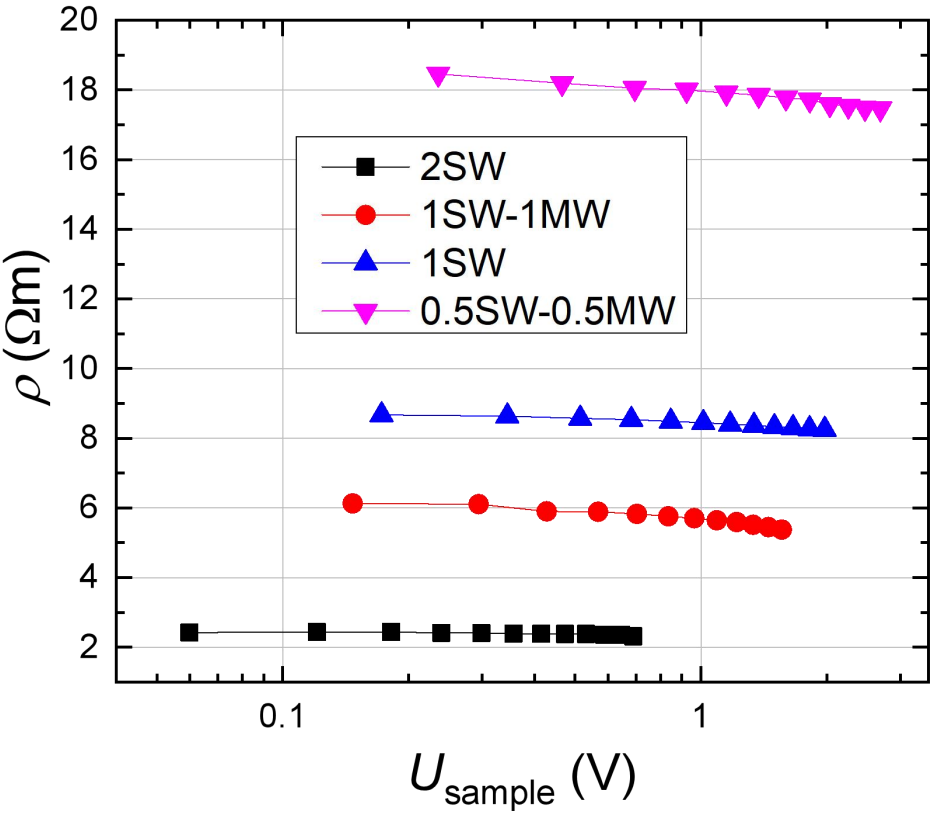

Figure 5.2.1. Dependence of the sample specific resistance on voltage of composites with different concentrations of fillers at room temperature.

It can be observed that the composite 2SW has the lowest specific resistance, and the 0.5SW-0.5MW has the highest. When the composite sample fillers are the same, but their concentrations are different, the specific resistance of the material decreases as the filler concentration increases. This result is to be expected, as higher concentrations of fillers naturally establish a more efficient percolation network within the material.

In the case of single-filler SWCNT composites, when the filler content is halved from 1 wt.% to 2 wt.%, the specific resistance of the composite increases from approximately 2.4 Ωm to 8.6 Ωm. In the case of hybrid composites with SWCNTs and MWCNTs as fillers, it can be observed that when the individual filler concentrations are doubled from 0.5 wt.% to 1 wt.%, the specific resistance of the composite increases from to approximately 6.1 Ωm to 18.4 Ωm. It shows that in the case of single-filler composites, when filler concentrations differ by two times, the absolute difference of specific resistance is lower than in the case of hybrid filler composites (6.2 Ωm versus 12.3 Ωm, respectively), but the relative difference is slightly higher (3.58 versus 3.02, respectively). This suggests that increasing the filler concentration in single-filler composites results in a more notable relative reduction of specific resistance.

When comparing single-filler and hybrid filler composites with equivalent total filler content, it can be observed that when the total filler concentration is higher (2SW and 1SW-1MW case), the absolute difference of specific resistance is lower (6.2 Ωm versus 12.3 Ωm, respectively), but the relative difference is higher (3.58 versus 3.02, respectively). This suggests that a higher absolute concentration of MWCNT correlates with a stronger impact on the specific resistance value.

In conclusion, the specific resistance of hybrid SWCNT/MWCNT composite samples is generally higher than that of single-filler SWCNT composite samples, and depends more strongly on voltage. This could be explained by the filler geometry. Individual MWCNTs are larger and therefore heavier than SWCNTs, as described in Section 3. Since the composite filler content is given by weight, the same weight content of MWCNTs occupy a smaller volume in the composite sample than SWCNTs. This means that the average distance between filler particles becomes larger, which leads to an increase in specific resistivity.

5.2.2. Voltage Fluctuations at Room Temperature

At room temperature, the low frequency noise of the composite samples (voltage fluctuation spectral density) is generally of 1/f type. An example of spectra observed during the study is given in Figure 5.2.2 for composite sample 1SW. The spectra given are characteristic of the type of spectra observed for the other composite samples in this study. Figure 5.2.2 also shows the level and spectra of the noise that is produced by the measurement system (dark grey points).

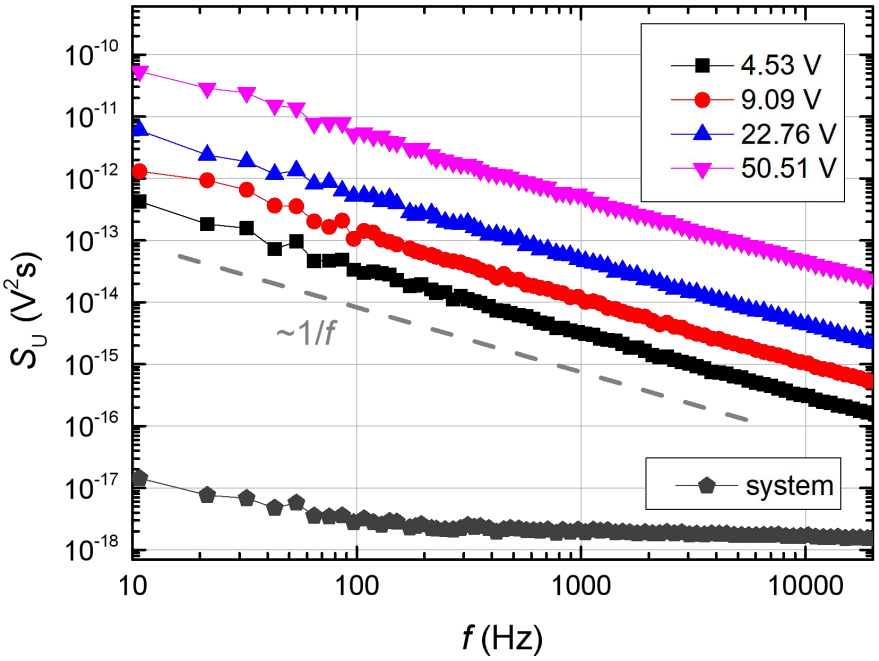

Figure 5.2.2. Dependence of the noise spectral density on voltage at room temperature (sample 1SW).

The dependence of the voltage noise spectral density on voltage for composite CNT with different concentration at room temperature is shown by Figure 5.2.3. The composite voltage noise spectral density is divided by the voltage square to more easily identify the value of b. The exponent b = 2 is characteristic of resistance fluctuations due to processes of generation and recombination of charge carriers.

The trendline of composite samples 0.5SW-0.5MW and 1SW are almost flat, which means that the spectral density of noise increases quadratically with increasing sample voltage. This means that in these composites, the origin of noise is related to resistive fluctuations in the material, which means the noise may be due to the generation and recombination of charge carriers inside the material. In this case, as the sample voltage increases, the contribution of resistive fluctuations to the noise increases, which leads to a quadratic increase in the noise spectral density.

Conversely, the trendlines of composite 2SW and 1SW-1MW are trending downwards. This relationship means that the spectral density of noise increases more linearly with increasing sample voltage. This situation is often related to tunneling processes in the material, so tunneling may cause a linear increase in the noise spectral density as the sample voltage increases.

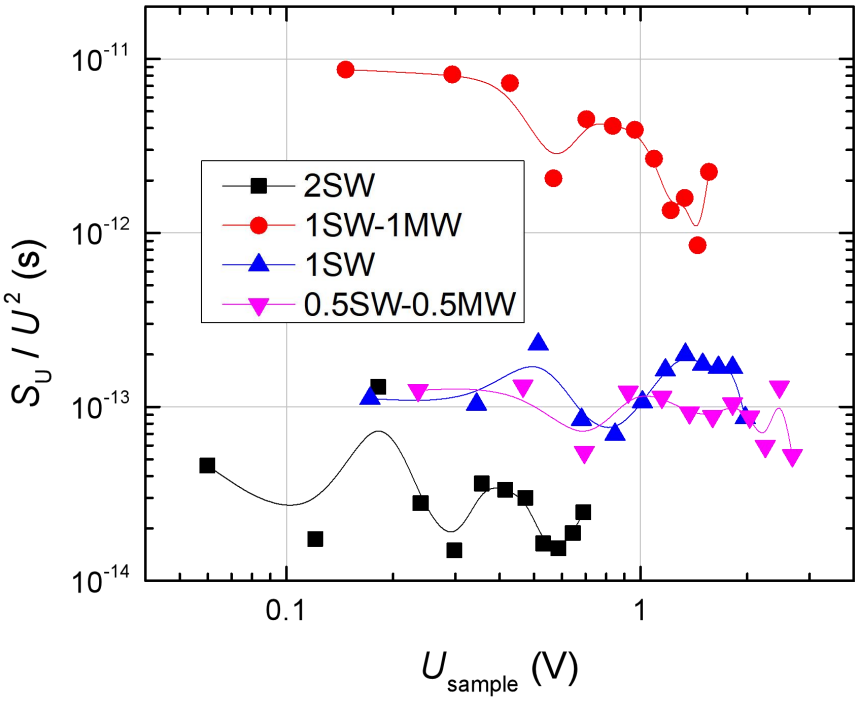

Figure 5.2.3. Dependence of the voltage noise spectral density on voltage of composites with different concentrations of fillers at room temperature (968 Hz).

5.2.3. Characteristics Dependence on Temperature

Figure 5.2.4 shows the temperature dependence of the resistivity for CNT/polymer composites containing different types and concentrations of carbon nanotubes. All samples exhibit a negative temperature coefficient of resistivity over the investigated temperature range (75–365 K), indicating that charge transport is dominated by thermally activated processes rather than metallic conduction along individual nanotubes.

The composite sample 2SW shows the lowest resistivity, consistent with a well-developed percolation network and a large number of parallel conductive pathways. However, the specific resistance composite sample also shows some instability at low temperatures.

In contrast, the composite sample 0.5SW-0.5MW exhibits the highest resistivity and the strongest temperature dependence, suggesting that charge transport is governed by tunneling across CNT–CNT junctions close to the percolation threshold and the concentration of filler in the 0.5SW-0.5MW is lowest, that affects the specific resistivity changing the most with temperature.

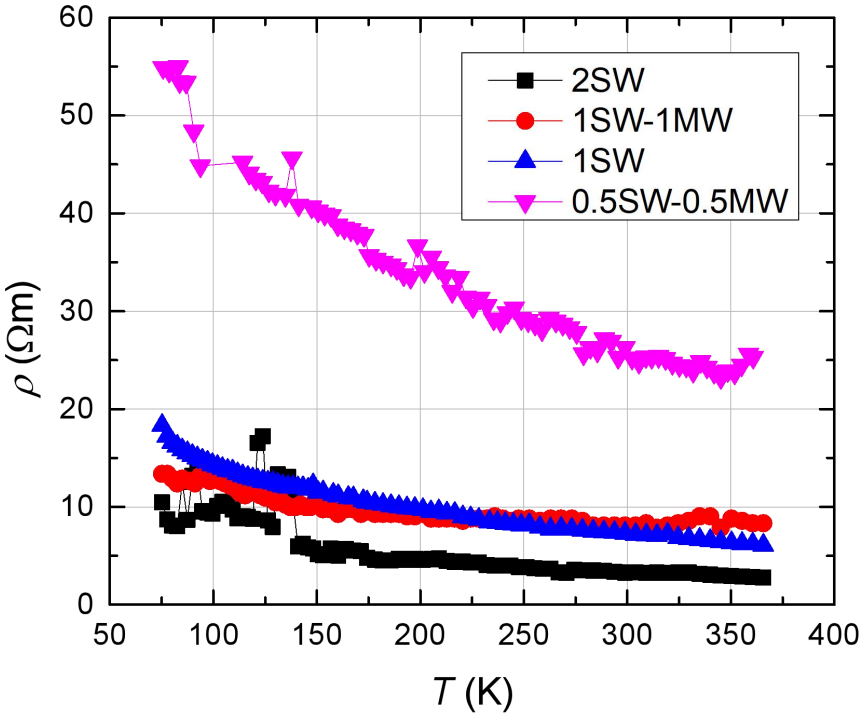

Figure 5.2.4. Dependence of specific resistance of composites with different concentrations of fillers on temperature (U = 9.2 V).

Figure 5.2.5 shows the Arrhenius plots of the resistivity for the 1SW and the 0.5SW-0.5MW composites in the form of ln(ρ) versus 1000/T. In both composite samples, the temperature dependence of resistivity can be divided into two distinct linear regimes, indicating the presence of multiple thermally activated charge transport processes.

At lower temperatures (higher 1000/T), the resistivity follows an Arrhenius dependence, but with lower activation energies. The activation energy (E_A) is defined as the minimum energy required to start the electrical conduction process [33]. The activation energies at lower temperatures E_{A1} are ~61 meV for 1SW and ~58 meV for 0.5SW-0.5MW, the temperature intervals of the regimes are 80.2 – 145.8 K for 1SW and 83.1 – 172.7 K for 0.5SW-0.5MW, respectively. In this region, charge transport is primarily dominated by a limited number of low-barrier carbon nanotube-carbon nanotube junctions, corresponding to shorter tunneling distances or more favorable contacts within the conductive network. As the temperature decreases, only the lowest-energy pathways remain active, leading to a decrease in the effective activation energy [34].

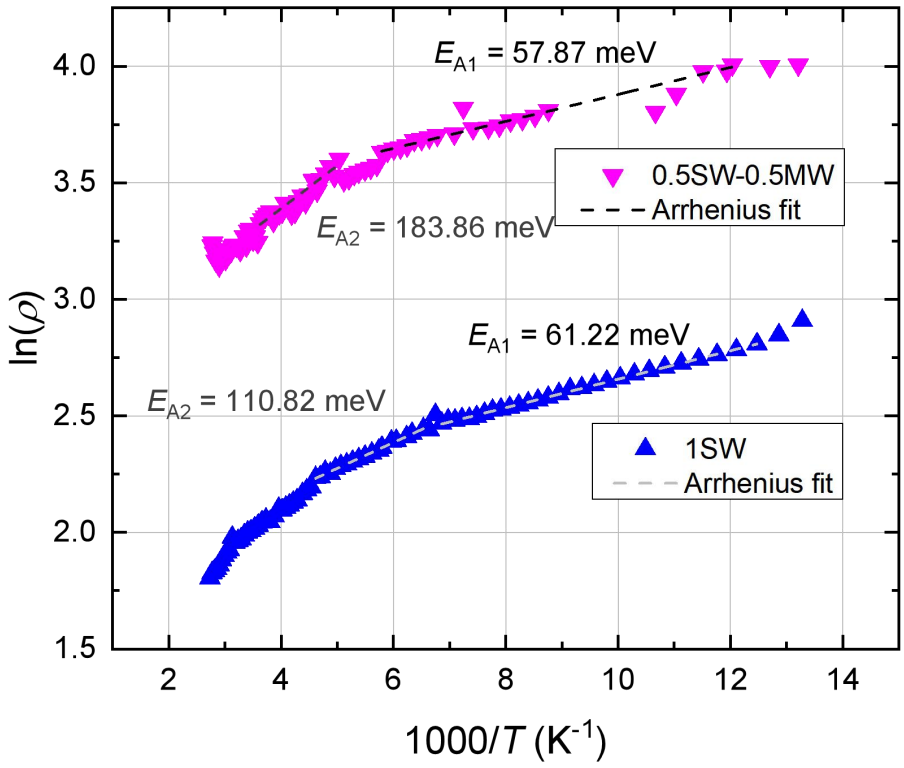

Figure 5.2.5. Temperature dependence of resistivity for samples of 0.5SW-0.5MW and 1SW. Symbols are experimental data points. Dashed lines are the Arrhenius fit.

At higher temperatures (lower than 1000/*T*), a second Arrhenius region emerges with a larger activation energy E_{A2} emerges (~111 meV for 1SW and ~184 meV for 0.5SW-0.5MW). The temperature intervals of E_{A2} are 153.1 - 216.7 K for 1SW and 198.7 - 275.5 K for 0.5SW-0.5MW respectively. This larger activation energy does not necessarily mean that individual charge carriers require more energy to transition; rather, it reflects the gradual participation of more CNT-CNT junctions with higher barriers in the reaction as thermal energy increases. The activation of these additional junctions with lower barriers results in a steeper temperature dependence of resistivity and an increased apparent activation energy [34].

Notably, the mixed 0.5SW-0.5MW composite exhibits a significantly higher E_{A2} compared to the 1SW sample, suggesting the influence of different types and weights of fillers. Because MWCNTs are heavier than SWCNTs, samples containing MWCNTs will have fewer CNTs than samples containing only SWCNTs, given the same filler weight ratio. This means that for 0.5SW-0.5MW, fewer CNTs are involved in conductivity, thus increasing the potential barrier.

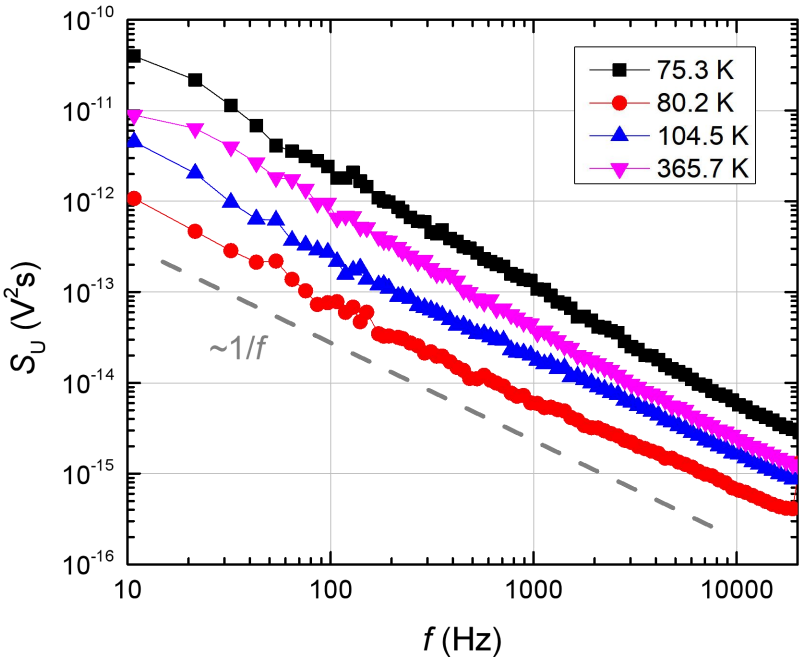

Figure 5.2.6. Dependence of the noise spectral density on temperature (U = 9.2 V, sample 1SW).

The low frequency noise of the composite samples observed during the temperature characteristics study is also generally of 1/f type. An example of spectra observed during the study is given in Figure 5.2.6 for composite sample 1SW. The spectra given are characteristic of the type of spectra observed for the other composite samples in this study. Since 1/f noise can be understood as a superposition of many individual generation-recombination events with a wide distribution of lifetimes, this result means that noise in the composites is not caused by select specific defects [18].

Figure 5.2.7 presents the temperature dependence of the normalized voltage noise spectral density S_U/U^2 measured at a fixed frequency 985 Hz in the $1/f$ noise regime. All samples exhibit pronounced low frequency noise, characteristic of conductance fluctuations in percolating CNT networks.

The composite sample 1SW-1MW shows the highest noise level over the entire temperature range, despite its moderate resistivity, indicating that a small number of fluctuating CNT–CNT junctions dominate the overall conductance. The differences in normalized voltage noise in the studied composite samples can also be attributed to the different geometries of the carbon nanotube fillers. Single-walled carbon nanotubes (SWCNTs) have smaller diameters and higher aspect ratios, resulting in smaller effective contact areas and greater fluctuations in tunneling distances, making the final conductive network more susceptible to conductivity fluctuations. In contrast, multi-walled

carbon nanotubes (MWCNTs) have larger diameters and multiple concentric shells, providing more stable inter-tube contacts and partially parallel conductive paths.

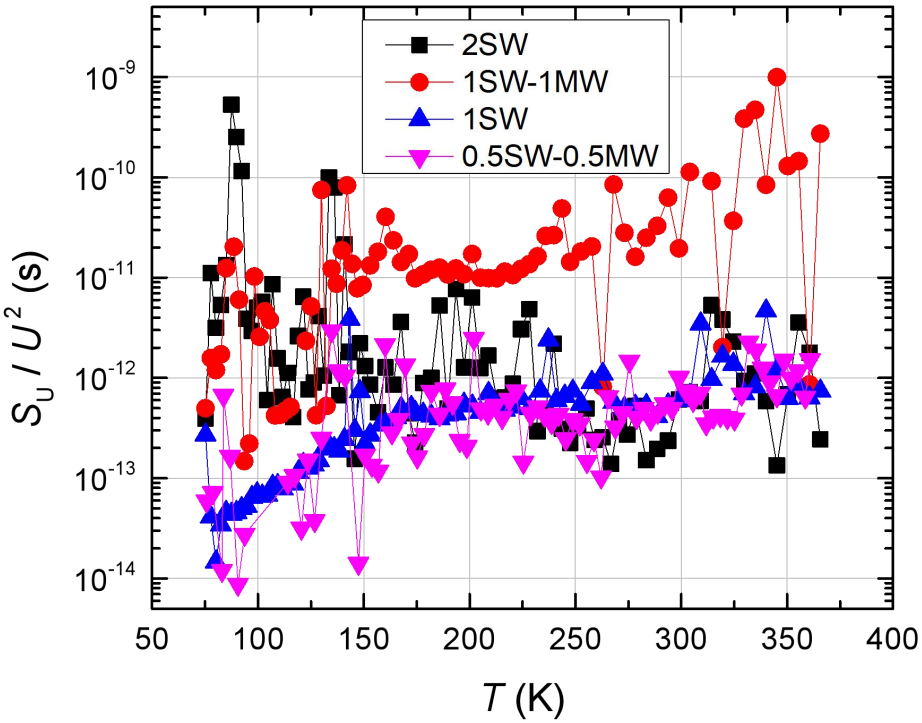

Figure 5.2.7. Dependence of normalized voltage noise spectral density on temperature (968 Hz, $U = 9.2$ V).

In SWCNT/MWCNT hybrid composites, the geometrical differences between the two nanotube types lead to a widespread distribution of heterojunctions, some of which become critical bottlenecks for charge transport. Fluctuations at these geometrically unfavorable heterojunctions are significantly amplified near the percolation threshold, resulting in enhanced low frequency noise. The enhanced noise in mixed CNT systems is attributed to the increased heterogeneity of tunneling junctions between different types of nanotubes. These results demonstrate that low-frequency noise is highly sensitive to the microscopic structure of the conductive network and provides complementary information to conventional resistivity measurements.

It should be pointed out that all composite samples exhibit higher noise level at approximately 150 K. That is due to the studied temperature range covers the glass transition temperature of the PDMS matrix ($T_g \approx 150-170$ K). Below T_g, the polymer chains are in a glassy state, forming relatively stable CNT-CNT connections. Above T_g, the transition from the glassy to the rubbery state causes changes within the material, leading to increased noise.

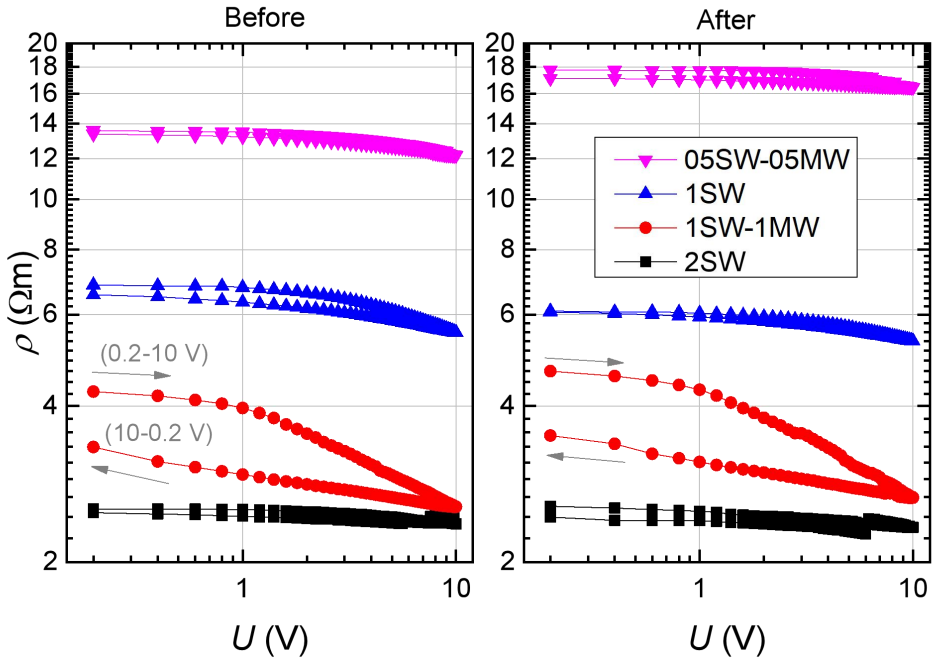

Figure 5.2.8. Comparison of dependency of specific resistance of composites on voltage before and after temperature characteristic measurements.

A comparison of the dependency of specific resistance of composites on voltage before and after the temperature characteristic measurement (essentially, one cooling and heating cycle) is shown in Figure 5.2.8. All composite samples exhibit a decrease in resistivity with increasing applied voltage. The specific resistance of composite sample with hybrid filler (0.5SW-0.5MW and 1SW-1MW) increased after temperature measurement, the specific resistance of the composite sample 1SW slightly decreased, and the specific resistance of the composite sample 2SW did not exhibit a notable change.

This figure also demonstrates that the specific resistance of the composite sample 2SW shows some instability around the 9 V region, which is slightly more pronounced after the temperature cycling. This could relate to the instability that was seen in the specific resistivity of this sample at low temperature (Figure 5.2.4). Also, it can be observed that when voltage is swept from 0.2 V to 10 V and then back to 0.2 V, composite specific resistance is slightly decreased, and this effect is more pronounced for the composite samples with MWCNT. This result highlight the CNT network topology in the composite sample impact the specific resistance of composites

Conclusions

1. The specific resistance and low frequency noise level of composite samples obtained from the top section of the material is higher and more variable than the resistivity and noise level of composite samples obtained from the side section of the material. The uneven set down of CNTs leads to the different distribution of the filler, which causes the higher resistivity and low frequency noise level of composite samples obtained from the top section.

2. The specific resistance of hybrid SWCNT/MWCNT composites is generally higher than that of single-filler SWCNT composites for the same total filler concentration by weight. Since individual MWCNTs are larger and therefore heavier than SWCNTs, the same weight content of MWCNTs occupy a smaller volume in the composite, so the average distance between filler particles is greater.

3. Composite sample low frequency noise is predominantly $1/f$ type. For composite samples with lower total filler content, voltage noise spectral density is proportional to the voltage square, characteristic of noise arising from resistance fluctuations. For composite samples with higher total filler content, the proportionality to voltage becomes more linear, which is characteristic of more tunneling processes.

4. The specific resistance of samples is inversely proportional to the temperature. The normalized voltage noise spectral density of samples is proportional to the temperature. The temperature dependence of resistivity for samples of 0.5SW-0.5MW and 1SW follows an Arrhenius dependence, which means charge carrier transport is thermally activated.

Vilniaus universitetas Fizikos fakultetas
Taikomosios Elektrodinamikos ir Telekomunikacijų institutas
Zifan Wang

Hibridinių kompozitų su anglies nanodalelėmis triukšminė spektroskopija

Magistro baigiamasis darbas

Santrauka

Šio darbo tikslas yra ištirti polidimetilsiloksano (PDMS) matricos kompozitų su vienasienių (SWNCT) ir daugiasienių (MWCNT) anglies nanodalelių užpildais varžines ir žemo dažnio triukšmo charakteristikas.

Tyrimas sudarytas iš dviejų dalių. Pirmoje tyrimo dalyje lyginami skirtingų dydžių, tos pačios sudėties kompozitiniai bandiniai, pagaminti iš skirtingų kompozitinės medžiagos sričių. Antroje tyrimo dalyje tiriami vienfaziai SWCNT bei daugiafaziai SWCNT/MWCNT kompozitai su skirtingomis užpildų koncentracijomis. Savitosios varžos ir žemo dažnio triukšmo (10 Hz – 20 kHz) tyrimai atlikti kambario temperatūroje, įtampos intervale nuo 4,5 V iki 55 V, bei keičiant kompozitinio bandinio temperatūrą intervale nuo 75 K iki 365 K esant pastoviai 9,2 V įtampai.

Kompozitinių bandinių, pagamintų iš medžiagos viršutinės srities, savitoji varža ir žemo dažnio triukšmas yra didesni ir labiau nesutampantys tarpusavyje nei bandinių, pagamintų iš medžiagos skerspjūvio. Dėl didesnio anglies nanovamzdelių nusėdimo medžiagos apačioje, užpildo pasiskirstymas medžiagos tūryje yra nevienodas.

Daugiafazių SWCNT/MWCNT kompozitų savitoji varža yra didesnė nei atitinkamos suminės svorio koncentracijos vienfazių SWCNT kompozitų. Dėl didesnių MWCNT matmenų, analogiška MWCNT svorio koncentracija užima mažesnį tūrį kompozite, dėl ko vidutiniai atstumai tarp užpildo dalelių yra didesni.

Kompozitų žemo dažnio triukšmas yra 1/f tipo. Kompozitų su mažesnėmis užpildo koncentracijomis įtampos fliuktuacijų spektrinis tankis yra proporcingas įtampos kvadratui: jų triukšmas yra kylantis dėl varžos fliuktuacijų. Kompozitų su didesnėmis užpildo koncentracijomis įtampos fliuktuacijų spektrinis tankis yra proporcingas įtampai: jų triukšmas yra kylantis dėl tuneliavimo reiškinių.

Kompozitų savitoji varža atvirkščiai priklauso nuo temperatūros. Kompozitų normuotas įtampos fliuktuacijų spektrinis tankis priklauso nuo temperatūros. Kompozitų su mažesnėmis užpildo koncentracijomis savitajai varžai taikytinas Arenijaus šiluminės aktyvacijos modelis.

References

[1] Melk, L. (2016). Processing and properties of zirconia-CNT composites (Doctoral dissertation, Luleå tekniska universitet).

[2] Tretjak, M., Palaimiene, E., Pralgauskaitė, S., Matukas, J., Banys, J., Macutkevič, J., ... & Celzard, A. (2021). Noise and Electrical Characteristics of Composites Filled with Onion-Like Carbon Nanoparticles. Polymers, 13(7), 997. DOI: 10.3390/polym13070997

[3] Marulanda, J. M. (Ed.). (2011). Carbon Nanotubes: Applications on Electron Devices. InTech, Aug. 01, 2011. DOI: 10.5772/977

[4] Li, Q. W., Li, Y., Zhang, X. F., Chikkannanavar, S. B., Zhao, Y. H., Dangelewicz, A. M., ... & Zhu, Y. T. (2007). Structure-dependent electrical properties of carbon nanotube fibers. Advanced Materials, 19(20), 3358-3363. DOI: 10.1002/adma.200602966

[5] Fischer, J. E. (2006). Carbon nanotubes: Structure and Properties. In Nanotubes and Nanofibers, 1(1). ISBN-10: 0849393876

[6] Manikandan, N., VP, S. K., Rathis, G., & Shabariganesh, T. K. (2021). Carbon nanotubes and their properties-The review. Materials today: Proceedings, 47, 4682-4685. DOI: 10.1016/j.matpr.2021.05.543

[7] Spitalsky, Z., Tasis, D., Papagelis, K., & Galiotis, C. (2010). Carbon nanotube–polymer composites: chemistry, processing, mechanical and electrical properties. Progress in polymer science, 35(3), 357-401. DOI: 10.1016/j.progpolymsci.2009.09.003

[8] Devaux, E., Koncar, V., Kim, B., Campagne, C., Roux, C., Rochery, M., & Saihi, D. (2007). Processing and characterization of conductive yarns by coating or bulk treatment for smart textile applications. Transactions of the Institute of Measurement and Control, 29(3-4), 355-376. DOI: 10.1177/0142331207081726

[9] Das, R., Shahnavaz, Z., Ali, M. E., Islam, M. M., & Abd Hamid, S. B. (2016). Can we optimize arc discharge and laser ablation for well-controlled carbon nanotube synthesis?. Nanoscale research letters, 11, 1-23. DOI: 10.1186/s11671-016-1730-0

[10] Nurazzi, N. M., Sabaruddin, F. A., Harussani, M. M., Kamarudin, S. H., Rayung, M., Asyraf, M. R. M., ... & Khalina, A. (2021). Mechanical performance and applications of CNTs

reinforced polymer composites—A review. Nanomaterials, 11(9), 2186. DOI: 10.3390/nano11092186

[11] Byrne, M. T., & Gun'ko, Y. K. (2010). Recent advances in research on carbon nanotube–polymer composites. Advanced materials, 22(15), 1672-1688. DOI: 10.1002/adma.200901545

[12] Liang, X., & Cheng, Q. (2018). Synergistic reinforcing effect from graphene and carbon nanotubes. Composites Communications, 10, 122-128. DOI: 10.1016/j.coco.2018.09.002

[13] Peng, C., Zhang, S., Jewell, D., & Chen, G. Z. (2008). Carbon nanotube and conducting polymer composites for supercapacitors. Progress in Natural science, 18(7), 777-788. DOI: 10.1016/j.pnsc.2008.03.002

[14] Qin, Jinqi & Lu, Hongwei & Yang, Shijia & Su, Weitao & Xing, Yu. (2024). Research Progress in Dielectric Properties of Inorganic Two-Dimensional Nano-Fillers Polyvinylidene Fluoride Nano-Dielectric Materials. Energy Technology. 12. DOI: 10.1002/ente.202400967.

[15] Stallinga, P. J. A. M. (2011). Electronic transport in organic materials: Comparison of band theory with percolation/(variable range) hopping theory. Advanced Materials, 23(30), 3356-3362. DOI: 10.1002/adma.201101129

[16] Mireckas, Frydrichas & Korzhenevskaya, Marina & Pralgauskaitė, Sandra & Matukas, Jonas & Meisak, Darya & Gaidukovs, Sergejs & Macutkevic, Jan & Banys, J.. (2023). Low Frequency Noise and Synergy Effect in Hybrid Composites with Carbon Nanoparticles. 1-4. DOI: 10.1109/ICNF57520.2023.10472743.

[17] Bao, W. S., Meguid, S. A., Zhu, Z. H., & Weng, G. J. (2012). Tunneling resistance and its effect on the electrical conductivity of carbon nanotube nanocomposites. Journal of Applied Physics, 111(9). DOI: 10.1063/1.4716010

[18] Balandin, A. A. (2013). Low-frequency 1/f noise in graphene devices. Nature nanotechnology, 8(8), 549-555. DOI: 10.1038/nnano.2013.144

[19] Van der Ziel, A. (1979). Flicker noise in electronic devices. In Advances in electronics and electron physics (Vol. 49, pp. 225-297). Academic Press. DOI: 10.1016/S0065-2539(08)60768-4

[20] Popescu, S., Lozneanu, E., & Sanduloviciu, M. (2003). Self-organized complex space charge configurations at the origin of flicker noise. Chaos, Solitons & Fractals, 17(2-3), 203-207. DOI: 10.1016/S0960-0779(02)00342-9

[21] Salvadé, Y., & Dändliker, R. (2000). Limitations of interferometry due to the flicker noise of laser diodes. JOSA A, 17(5), 927-932. DOI: 10.1364/JOSAA.17.000927

[22] Simoen, E., & Claeys, C. (1999). On the flicker noise in submicron silicon MOSFETs. Solid-State Electronics, 43(5), 865-882. DOI: 10.1016/s0038-1101(98)00322-0

[23] Zhuang, Y., Chen, T., Chaganti, S., & Chen, D. (2015, August). Effect of flicker noise on SEIR for accurate ADC linearity testing. In 2015 IEEE 58th International Midwest Symposium on Circuits and Systems (MWSCAS) (pp. 1-4). IEEE. DOI: 10.1109/MWSCAS.2015.7282187

[24] Lukyanchikova, N., Garbar, N., Petrichuk, M., Simoen, E., & Claeys, C. (2000). Flicker noise in deep submicron nMOS transistors. Solid-State Electronics, 44(7), 1239-1245. DOI: 10.1016/S0038-1101(00)00039-3

[25] Palenskis, V.; Matukas, J.; Glemža, J.; Pralgauskaitė, S. (2022) Review of Low-Frequency Noise Properties of High-Power White LEDs during Long-Term Aging. Materials, 15, 13. DOI: 10.3390/ma15010013

[26] Welker, J., de Faria Elsner, F., & Giessibl, F. J. (2011). Application of the equipartition theorem to the thermal excitation of quartz tuning forks. Applied Physics Letters, 99(8). DOI: 10.1063/1.3627184.

[27] Collins, P. G., Fuhrer, M. S., & Zettl, A. (2000). 1/f noise in carbon nanotubes. Applied Physics Letters, 76(7), 894-896. DOI: 10.1063/1.125621.

[28] Merchant, C. A., & Marković, N. (2009). Current and shot noise measurements in a carbon nanotube-based spin diode. Journal of Applied Physics, 105(7). DOI: 10.1063/1.3072020.

[29] Chaste, J., Pallecchi, E., Morfin, P., Fève, G., Kontos, T., Berroir, J. M., ... & Plaçais, B. (2010). Thermal shot noise in top-gated single carbon nanotube field effect transistors. Applied Physics Letters, 96(19). DOI: 10.1063/1.3425889.

[30] The Dow Chemical Company. SYLGARD™ 184 Silicone Elastomer Technical Data Sheet. <https://www.dow.com/content/dam/dcc/documents/en-us/productdatasheet/11/11-31/11-3184-sylgard-184-elastomer.pdf> [accessed 2026-04-30].

[31] US Research Nanomaterials, Inc. Research Grade Super High Purity SWCNTs. <https://www.us-nano.com/inc/sdetail/378> [accessed 2026-04-30].

[32] US Research Nanomaterials, Inc. MWCNTs <https://www.us-nano.com/inc/sdetail/224> [accessed 2026-04-30].

[33] Abu Saleh B A, Ramadin Y, Zihlif A M, et al. (2016) Optical and electrical properties of polystyrene composites containing ultrafine iron particles. Journal of Thermoplastic Composite Materials, 29(2): 204-218. DOI: 10.1177/0892705714526914.

[34] Sheng P. (1980) Fluctuation-induced tunneling conduction in disordered materials. Physical Review B, 21(6): 2180. DOI: 10.1103/PhysRevB.21.2180.